MATERIALS CHEMISTRY FRONTIERS

RESEARCH ARTICLE

View Article Online
View Journal | View Issue

Cite this: *Mater. Chem. Front.*, 2025, **9**, 2224

Doping PEDOT:PSS with cesium chloride for enhancing the performance of perovskite solar cells

Wan Cheng,†[ab] Cunyun Xu,†[c] Ying Li,[ab] Yanqing Yao,[a] Yuanlin Yang,[ab] Xusheng Zhao,[a] Ping Li*[a] and Lijia Chen*[b]

Received 12th February 2025,
Accepted 19th May 2025

DOI: 10.1039/d5qm00131e

rsc.li/frontiers-materials

Poly(3,4-ethylenedioxythiophene):poly(styrene sulfonate) (PEDOT:PSS) is the most commonly used hole transport layer (HTL) material in perovskite solar cells (PSCs) due to its high visible light transmittance, excellent solution processability, and wettability suitable for top perovskite formation. The presence of surface defects in PEDOT:PSS films decreases the photoelectric conversion efficiency (PCE) and long-term stability of PSCs. These defects lead to the formation of pores in the growth of perovskite films on PEDOT:PSS, impeding the extraction and transfer of effective charges. Therefore, in this article, cesium chloride is doped into PEDOT:PSS to enhance its surface morphology, reduce surface roughness, improve the quality of sulfide thin films, promote charge transfer ability between interfaces, enhance conductivity, reduce non radiative recombination of the device, and improve the photovoltaic performance of the device. The open circuit voltage (V_{OC}) increased from 1.00 V to 1.02 V, the short-circuit current (J_{SC}) increased from 21.04 mA cm^{-2} to 21.72 mA cm^{-2}, the fill factor (FF) increased from 77.90% to 82.04%, and the PCE of $MAPbI_{3-x}Cl_x$ PSCs increased from 16.39% to 18.18%. Specifically, when using cesium chloride-doped PEDOT:PSS as the HTL, the PCE of the Sn-Pb PSCs increased from 19.49% to 21.44%.

1 Introduction

Because of the high absorption coefficient, long diffusion length, and high carrier mobility, organic–inorganic hybrid perovskites are frequently utilized in light-emitting diodes, photodetectors, and perovskite solar cells (PSCs).[1–7] Since its initial report in 2009, the photoelectric conversion efficiency (PCE) of PSCs has increased dramatically. At this time, it is extremely similar to conventional monocrystalline silicon solar cells. Therefore, PSCs have great potential for commercialization in the future.[8–11] The hole transport layer (HTL) plays an important role in PSCs, and commonly used HTL PEDOT:PSS is one of the most widely used hole transport materials in the HTL of PSCs due to its advantages of low-temperature preparation, low cost, and high transparency.[12–16]

However, PEDOT:PSS has issues with conductivity and acidity.[17–20] Researchers have conducted many studies to try to solve these issues. Zhao *et al.*[21] prepared potassium thiocyanate (KSCN) film by adding KSCN to a PEDOT:PSS solution diluted with dihydrate in a volume ratio of 1 : 1. By inhibiting charge recombination, promoting carrier transport, lowering the hysteresis effect in PSCs, and increasing the electrical conductivity of HTLs made with the diluted PEDOT:PSS solution, the KSCN addition can improve device performance. Yang *et al.*[22] employed arginine as an additive in the PEDOT:PSS solution to adjust the pH value from 3.70 to 6.80. The inclusion of arginine improved the PCE from 15.06% to 17.35%. So, it is necessary to improve the surface morphology of PEDOT further: PSS will improve the quality of the chalcogenide film and the performance of PSCs. Consequently, it is essential to further enhance the surface morphology of PEDOT:PSS, as this will contribute to the improvement of the quality of the chalcogenide film and the performance of PSCs.[23]

This work describes the use of cesium chloride (CsCl) doping in PEDOT:PSS as an HTL for PSCs, which improves the surface morphology of PEDOT:PSS, increases the grain size of perovskite formed on PEDOT:PSS, and reduces non-radiative complexation, thus improving the charge transfer and extraction of perovskite to the HTL. In chalcogenide solar cells with the structure ITO/CsCl-PEDOT:PSS/$MAPbI_{3-x}Cl_x$/PCBM/BCP/Ag, the filling factor (FF) and photovoltaic conversion efficiency were successfully increased. For chalcogenide solar cells with the structure ITO/CsCl-PEDOT:PSS/$MAPbI_{3-x}Cl_x$/PCBM/BCP/Ag, the PCE and FF were successfully raised.

[a] *School of Physics and Electronic Science, Zunyi Normal University, Zunyi 563006, China. E-mail: lip19870212@126.com*
[b] *College of Physics and Electronic Engineering, Chongqing Normal University, Chongqing 401331, China. E-mail: ljchen01@cqnu.edu.cn*
[c] *Institute for Clean Energy and Advanced Materials, School of Materials and Energy, Southwest University, Chongqing 400715, China*
† Wan Cheng and Cunyun Xu contributed equally to this work.

In the meantime, the chalcogenide solar cell with the structure of ITO/CsCl-PEDOT:PSS/$(FASnI_3)_{0.6}(MAPbI_3)_{0.4}$/PCBM/BCP/Ag was also doped with CsCl in the PEDOT:PSS HTL. This resulted in a significant increase in the device's photovoltaic conversion efficiency and an improvement in its FF. According to the results, $MAPbI_{3-x}Cl_x$ and $(FASnI_3)_{0.6}(MAPbI_3)_{0.4}$ chalcogenide solar cells can both benefit from the use of CsCl doped PEDOT:PSS as an HTL, offering a straightforward and efficient technique.

2 Experiments

2.1. Materials

Lead iodide (PbI_2, 99.99%), formamidinium iodide (FAI, 99.90%), and tin(IV) iodide (SnI_2, 99.99%) were purchased from Advanced Election Technology Co., Ltd (China). Tin(II) fluoride (SnF_2, 99.00%) was purchased from Aladdin, and the lead thiocyanate ($Pb(SCN)_2$, 99.00%) was purchased from Sigma-Aldrich. Lead chloride ($PbCl_2$, 99.99%), methyl ammonium iodide (MAI, 99.50%), poly(3,4-ethylenedioxythiophene)polystyrene sulfonate (PEDOT:PSS (4083) 1.3–1.7%), [6,6]-phenyl C_{61} butyrate methyl ester ($PC_{61}BM$, 99.00%), bath copper (BCP, 99.00%) and silver (Ag, 99.99%) were purchased from Xi'an Polymer Light Technology Corp (China). Cesium chloride (CsCl, 99.00%), *N*,*N*-dimethylformamide (DMF, 99.90%), dimethyl sulfoxide (DMSO, 99.70%), chlorobenzene (CB, 99.90%), and ethanol (He, 99.90%) were purchased from J&K Scientific (China).

2.2. Sample preparation

Preparation of perovskite solar cell devices with ITO/CsCl-PEDOT:PSS/$MAPbI_{3-x}Cl_x$/PCBM/BCP/Ag and ITO/CsCl-PEDOT:PSS/$(FASnI_3)_{0.6}(MAPbI_3)_{0.4}$/PCBM/BCP/Ag structures.

(1) Preparation of the HTL: firstly, prepare PEDOT:PSS stock solution and deionized water in a volume ratio of 1 : 4 and filter for later use. Then, weigh 0 mg, 0.25 mg, 0.5 mg, and 0.75 mg of the corresponding cesium chloride and dissolve them in 1 mL of PEDOT:PSS solution to prepare CsCl PEDOT:PSS solutions with concentrations of 0 mg mL^{-1}, 0.25 mg mL^{-1}, 0.5 mg mL^{-1}, and 0.75 mg mL^{-1}, respectively. Use a pipette to transfer 40 μL of CsCl PEDOT:PSS solution of different concentrations at a speed of 6000 rpm onto four cleaned ITO substrates. After spin coating for 40 seconds, anneal at 130 °C for 20 minutes.

(2) $MAPbI_{3-x}Cl_x$ perovskite layer: the drugs MAI (222.30 mg), PbI_2 (580.90 mg) and $PbCl_2$ (38.90 mg) were weighed and dissolved in a solvent mixture of 1 mL of DMSO and DMF in a volume ratio of 9 : 1, and dissolved with stirring at room temperature to make a solution of perovskite precursor that was filtered and set aside. The prepared perovskite precursor solution (35 μL) was spin-coated onto the HTL at 400 rpm and 4000 rpm for 3 s and 30 s, respectively, and CB (80 μL) was dripped onto the substrate at the 12th s during the dynamic spin-coating process. The substrate was then heated on a heating stage at 50 °C for 2 min, followed by 30 min on a heating stage at 85 °C.

(3) Preparation of the $(FASnI_3)_{0.6}(MAPbI_3)_{0.4}$ perovskite layer: the drugs FAI (371.46 mg), SnI_2 (804.63 mg), MAI (228.90 mg), PbI_2 (663.86 mg), SnF_2 (33.84 mg), and $Pb(SCN)_2$ (46.56 mg) were weighed and dissolved in 1 mL of a DMF:DMSO mixture with a volume ratio of 4 : 1 and stirred overnight at room temperature, and filtered for later use. Then 35 μL of the perovskite precursor solution was pipetted and spun at 400 rpm for 3 s and then spun-coated at 6000 rpm for 30 s. During spin-coating, 80 μL of CB was pipetted and dripped onto the spinning substrate at the 15th s. The substrate was then heated for 2 min on a heating stage at 50 °C and then transferred to a heating stage at 85 °C for further heating for 30 min.

(4) Preparation of an electronic transport layer: to make a 20 mg mL^{-1} PCBM solution, weigh 20 mg of PCBM dissolved in 1 mL of CB; to make a 0.50 mg mL^{-1} BCP solution, weigh 0.50 mg of BCP dissolved in 1 mL of ethanol; filter and set aside. After the perovskite film was cooled to room temperature, 35 μL of 20 mg mL^{-1} PCBM solution was taken and spin-coated at 5000 rpm for 30 s. The substrate was then passed out of the glove box into a moisture-proof cabinet for 30 min for air oxidation. And then passed back into the glove box, and 35 μL of 0.50 mg mL^{-1} BCP solution was taken and spin-coated at 2000 rpm for 30 s on the PCBM film.

(5) Preparation of the silver electrode: the substrate was placed on a mask plate passed from the glove box to the vacuum chamber and 60 nm silver electrodes were deposited using thermal evaporation.

2.3. Device characterization

The current density voltage (*J*–*V*) characteristics are measured by a Keithley 2400 source measuring instrument under 100 mW cm^{-2} analog light (AM 1.50G). The roughness, crystal, and morphology characteristic of the film were investigated by atomic force microscopy (AFM, CSPM5500), an X-ray diffraction system (XRD, RigakuD/MAX2500PC) and field emission scanning electron microscopy (SEM, HITACHI Regulus8220), respectively. The absorption of perovskite thin films was tested using UV visible absorption spectroscopy (UV-8000S), and elemental studies were conducted using X-ray photoelectron spectroscopy (XPS Thermo Scientific™ Nexsa™). The steady-state photoluminescence (PL) spectra were measured with an LS-50B luminescence spectrometer (PerkinElmer). Electrochemical impedance spectroscopy (EIS) is obtained by applying a bias voltage of 0.80 V in the dark (model 660D, Shanghai Chenhua Instrument Co., Ltd, China). In the glove box, space charge limited current (SCLC), light intensity effect, and conductivity were measured using a Keithley 2400, while the dark current was tested in a dark environment.

3 Results and discussion

Cesium chloride-doped PEDOT:PSS was used as the HTL of the perovskite solar cell (the CsCl doping concentration of 0.50 mg mL^{-1} is noted as CsCl-PEDOT:PSS). To investigate whether CsCl is doped into the original PEDOT:PSS, X-ray

photoelectron spectroscopy (XPS) analysis was performed on PEDOT:PSS and CsCl-PEDOT:PSS, as shown in Fig. 1a. In the Cs(3d) orbital, no spurious peaks were detected in PEDOT:PSS, whereas CsCl-PEDOT:PSS showed two distinct characteristic peaks of $3d_{3/2}$ and $3d_{5/2}$ of the Cs element, which demonstrated that PEDOT:PSS was successfully doped with CsCl. In addition, the S(2p) and O(1s) orbitals of ITO/PEDOT:PSS and ITO/CsCl-PEDOT:PSS were also tested, as shown in Fig. 1b and c. After CsCl doping with PEDOT:PSS, the PEDOT and PSS chains underwent corresponding changes. For the S(2p) orbital, the S element in both the PEDOT and PSS chains shifted towards smaller binding energies. For the O(1s) orbital, the peak is divided into two parts; the higher binding energy is associated with PEDOT, and the lower binding energy is associated with PSS, and the O(1s) binding energy peak associated with PSS is shifted to the lower binding energy after CsCl modification.

To study the surface morphology of the films, AFM tests were performed on the PEDOT:PSS and CsCl-PEDOT:PSS hole-transporting layers, as shown in Fig. S1 (ESI†), the roughness of the PEDOT:PSS layer was 6.15 nm, and that of the CsCl-PEDOT:PSS was reduced to 4.21 nm, the reduction in surface roughness of the hole transport layer is beneficial for better contact between the perovskite layer and the PEDOT:PSS layer, thereby promoting the transport of electron hole pairs at the interface layer and further enhancing the carrier transport ability. To explore this conclusion, further tests were conducted on PEDOT:PSS/$MAPbI_{3-x}Cl_x$. The AFM of the CsCl-PEDOT:PSS/$MAPbI_{3-x}Cl_x$ layer, as shown in Fig. 2(a) and (b), shows that the roughness of the CsCl-PEDOT:PSS/$MAPbI_{3-x}Cl_x$ layer is 20.8 nm, which is lower than that of the PEDOT:PSS/$MAPbI_{3-x}Cl_x$ layer (24.4 nm). The results showed that the roughness of the doped perovskite film was significantly reduced, indicating that the doped PEDOT:PSS is more conducive to the crystallization of the perovskite, reducing the surface roughness of the perovskite layer and promoting the interface contact between the perovskite layer and the electron transport layer. The three-dimensional graphics of the perovskite film are shown in Fig. S2(a) and (b) (ESI†), which can more intuitively demonstrate that after cesium chloride doping, the crystallinity of the perovskite film is better, the surface of the film is smoother, and the charge transfer ability between the perovskite layer and other interface layers is promoted.

We utilized scanning electron microscopy (SEM) to characterize the morphology of perovskite films on PEDOT:PSS and cesium chloride-doped PEDOT:PSS substrates to be better examine the impact of cesium chloride-doped PEDOT:PSS on the morphology of the perovskites, as illustrated in Fig. 2c and d. After doping CsCl, the surface roughness of PEDOT:PSS decreases, and the defects and pores on the material surface decrease, directly leading to a reduction in non-radiative recombination centers, which reduces the non-radiative recombination of the device and enhances the carrier transport ability. The probability of them being captured decreases, resulting in a reduction in the capture cross-section. Fig. 2e and f represent the particle size analysis of the cesium chloride-doped perovskite film in PEDOT:PSS, which is more compact and uniformly structured. In comparison with PEDOT:PSS/$MAPbI_{3-x}Cl_x$ particles (311.01 nm), the particle size of CsCl-PEDOT:PSS/$MAPbI_{3-x}Cl_x$ is larger, being 330.64 nm. The single grain in the perovskite film can directly contact the HTL and the electron transport layer. The increase in grain size and crystal quality of the perovskite layer is beneficial for PSCs to better extract and transport electrons. Characterization of the XRD patterns of PEDOT:PSS/$MAPbI_{3-x}Cl_x$ and CsCl-PEDOT:PSS/$MAPbI_{3-x}Cl_x$ thin films is shown in Fig. S3 (ESI†). PEDOT:PSS/$MAPbI_{3-x}Cl_x$ and CsCl-PEDOT:PSS/$MAPbI_{3-x}Cl_x$ films exhibit characteristic peaks corresponding to the (110), (220), and (310) crystal planes at 14.14°, 28.48°, and 31.90°, indicating that the prepared films are indeed perovskite films with excellent crystallinity, which is in line with the SEM test results. Furthermore, following CsCl doping, the perovskite layer's UV visible absorption spectrum is essentially the same between 500 and 900 nm; Fig. 2g illustrates that the UV visible absorption spectrum of CsCl-PEDOT:PPS/$MAPbI_{3-x}Cl_x$ increases at 450 and 500 nm.

The steady-state PL of PEDOT:PSS/$MAPbI_{3-x}Cl_x$ and CsCl-PEDOT:PSS/$MAPbI_{3-x}Cl_x$ is presented in Fig. 2h. At the same excitation intensity, the PL intensity of CsCl-PEDOT:PSS/$MAPbI_{3-x}Cl_x$ is lower than that of PEDOT:PSS/$MAPbI_{3-x}Cl_x$. This indicates that after doping PEDOT:PSS with cesium chloride, the hole extraction rate of the interface layer significantly increases, the carrier transport ability is enhanced, and the electron hole recombination ability is reduced.[24,25]

Therefore, devices with the structure of ITO/CsCl-PEDOT:PSS/$MAPbI_{3-x}Cl_x$/PCBM/BCP/Ag, which were doped with CsCl at concentrations of 0 mg mL^{-1}, 0.25 mg mL^{-1}, 0.50 mg mL^{-1},

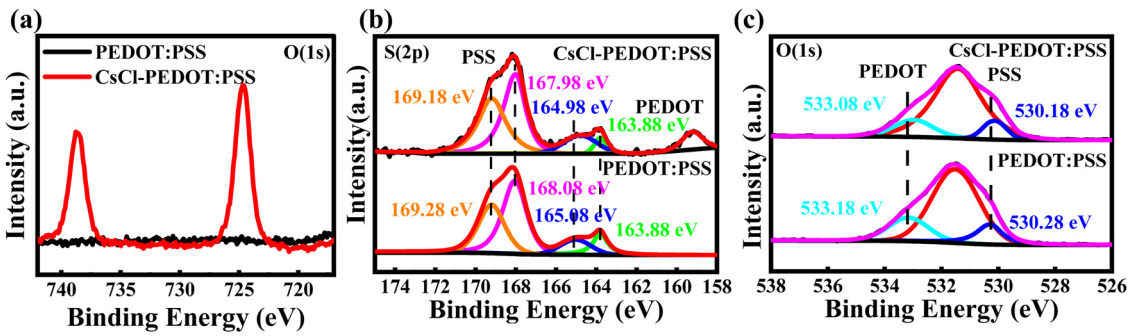

Fig. 1 High-resolution XPS spectra of (a) Cs(3d), (b) S(2p), and (c) O(1s) for the PEDOT:PSS and CsCl-PEDOT:PSS films.

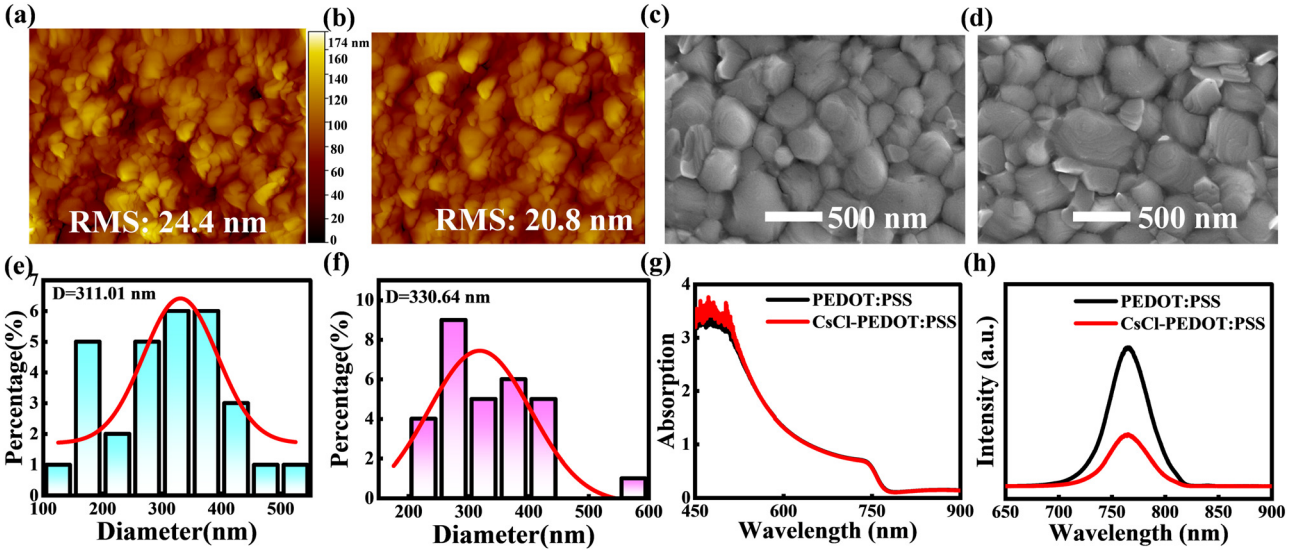

Fig. 2 AFM of (a) PEDOT:PSS/$MAPbI_{3-x}Cl_x$, and (b) CsCl-PEDOT:PSS/$MAPbI_{3-x}Cl_x$; SEM of (c) PEDOT:PSS/$MAPbI_{3-x}Cl_x$ structure, and (d) CsCl-PEDOT:PSS/$MAPbI_{3-x}Cl_x$; grain analysis of (e) PEDOT:PSS/$MAPbI_{3-x}Cl_x$, and (f) CsCl-PEDOT:PSS/$MAPbI_{3-x}Cl_x$; (g) ultraviolet absorption spectrum; (h) steady-state fluorescence spectrum.

and 0.75 mg mL^{-1}, were prepared separately, as illustrated in Fig. 3a. Their photoelectric performance was tested under AM 1.5G illumination at 100 mW cm^{-2}, and the *J–V* is shown in Fig. 3b and Table 1. The optimal performance of PEDOT:PSS PSCs is characterized by a PCE of 16.39%, an open circuit voltage (V_{OC}) of 1 V, a short-circuit current (J_{SC}) of 21.04 mA cm^{-2}, and a fill factor (FF) of 77.90%. The optimal performance of PEDOT:PSS doped with CsCl (doping concentration of 0.50 mg mL^{-1}) increased the PCE to 18.18%, the V_{OC} to 1.02 V, the J_{SC} to 21.72 mA cm^{-2}, and the FF to 82.04%.

Table 1 Performance parameters of inverted PSCs fabricated based on varying concentrations of CsCl

Device (mg mL^{-1})	V_{OC} (V)	J_{SC} (mA cm^{-2})	PCE (%)	FF (%)
0	1	21.04	16.39	77.90
0.25	1.02	22.38	17.84	78.16
0.5	1.02	21.72	18.18	82.04
0.75	1	21.31	17.09	80.20

To verify the feasibility and repeatability of the data, we prepared 20 sets of perovskite solar cell devices with CsCl doping concentrations of 0 mg mL^{-1}, 0.25 mg mL^{-1}, 0.50 mg mL^{-1}, and 0.75 mg mL^{-1} under the same conditions, and conducted data statistics on PCE, V_{OC}, J_{SC}, and FF, as shown in Fig. 4 and Table S1 (ESI†). It can be concluded that the performance of PSCs doped with CsCl at a PEDOT:PSS concentration of 0.50 mg mL^{-1} is optimal, with maximum PCE, V_{OC}, J_{SC} and FF values of 18.18%, 1.04 V, 22.26 mA cm^{-2}, and 82.04%, respectively. In contrast, the maximum PCE, V_{OC}, J_{SC}, and FF values of PEDOT:PSS devices are 16.39%, 1.02 V, 21.04 mA cm^{-2}, and 79.97%, respectively.

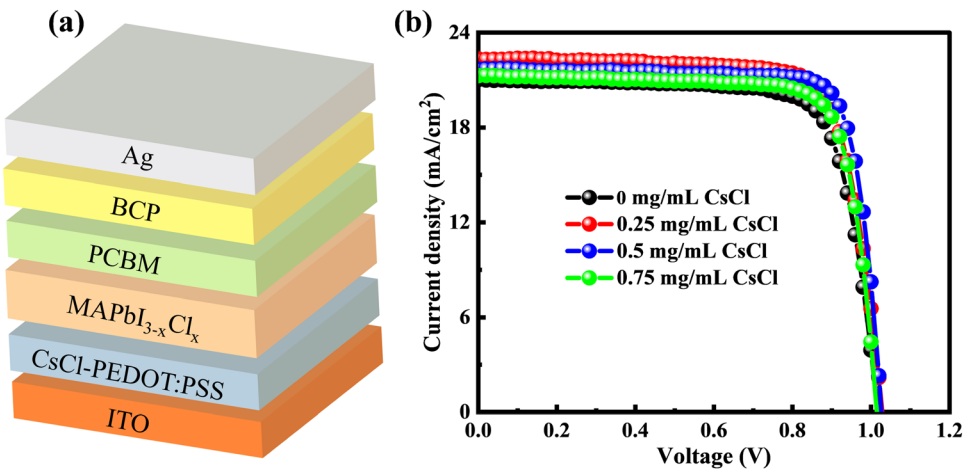

Fig. 3 (a) Device structure; (b) *J–V* curves of the best devices without and with CsCl.

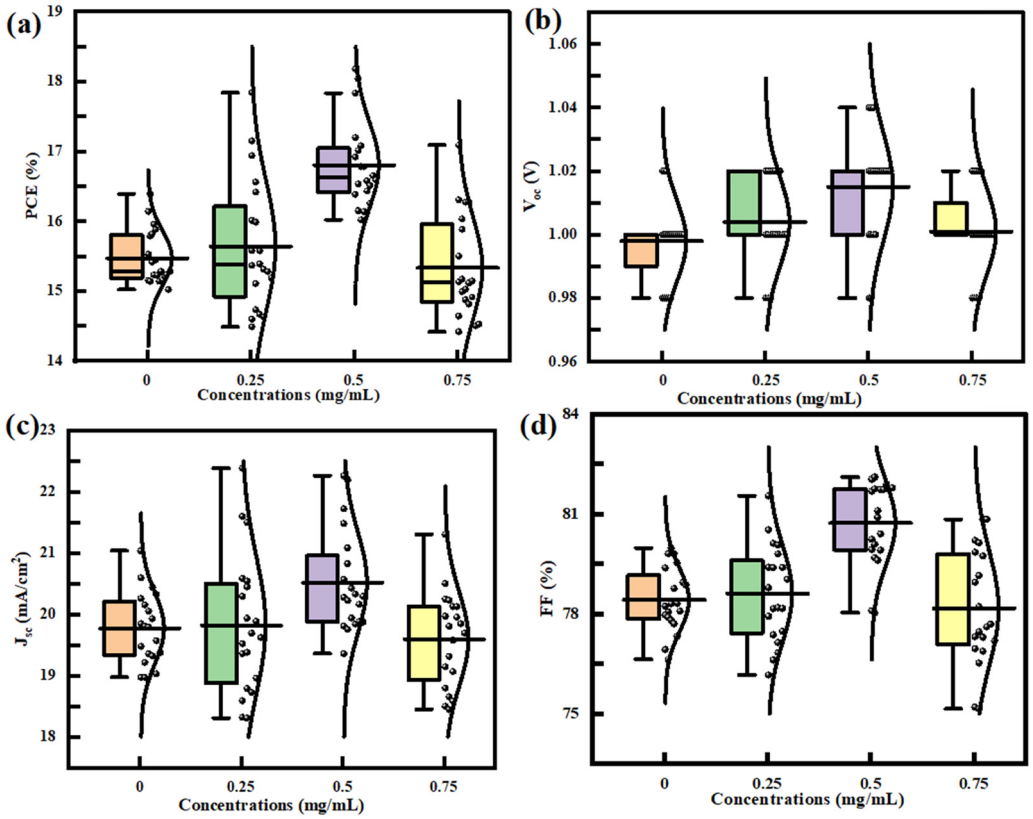

Fig. 4 Statistical analysis of the photovoltaic performance of 20 groups of devices for devices with potassium stearate concentrations of 0 mg, 0.25 mg, 0.5 mg, and 0.75 mg: (a) PCE; (b) V_{OC}; (c) J_{SC}; (d) FF.

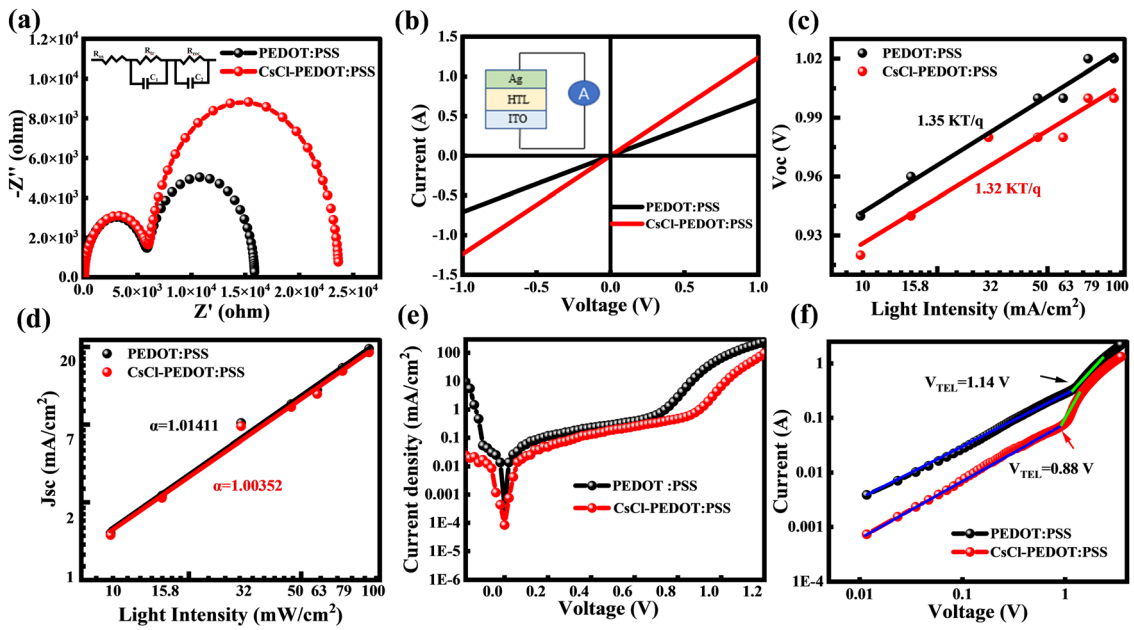

Fig. 5 (a) EIS measurements of the device (without and with CsCl) under dark conditions with a bias voltage of 0.80 V. The inset represents the corresponding equivalent circuit; (b) *I*–*V* curve with ITO/PEDOT:PSS/Ag and ITO/CsCl-PEDOT:PSS Ag structure; light intensity dependence of the PSCs without and with CsCl: (c) V_{OC} and (d) J_{SC}; (e) *J*–*V* curves of the device measured in the dark (without and with CsCl); (f) *J*–*V* curves based on ITO/PEDOT:PSS/$MAPbI_{3-x}Cl_x$/PTAA/Ag and ITO/CsCl-PEDOT:PSS/$MAPbI_{3-x}Cl_x$/PTAA/Ag.

The EIS of the PSCs was measured to investigate the charge recombination of PSCs devices. The corresponding Nyquist plot and equivalent circuit (inset) are shown in Fig. 5a, where R_{tr} represents the transfer resistance and R_{rec} represents the recombination resistance. The CsCl-doped device has the same transfer resistance as the original device, but its composite resistance value is significantly higher than that of the original device. When the composite resistance increases, it indicates that the charge recombination rate of the device decreases, the nonradiative recombination ability weakens, and the carrier transport ability of the device increases. At the same time, the electrical properties of the devices with structures of ITO/PEDOT:PSS/Ag and ITO/CsCl-PEDOT:PSS/Ag were tested, and their *J–V* curves are shown in Fig. 5b. The conductivity of the devices doped with CsCl is higher compared to the original device, and higher conductivity is conducive to charge extraction and transmission, consistent with impedance spectroscopy analysis. The increase in conductivity indicates that in doped devices, more electrons can be excited into the conduction band, resulting in an increase in electron density of states. There are more available states in the energy band to accommodate additional electrons, thereby enhancing the electron capture ability and promoting effective charge extraction and transfer. At the same time, the reduction of surface defects in the SEM images also confirms this fact. When the defects decrease, the electron affinity increases and the PCE improves. The increase in electron affinity makes it easier for electrons to be extracted rather than captured, further reducing the occurrence of non-radiative recombination.

The defects within the device can influence the charge transfer and recombination of photo-generated carriers. To further investigate the defect-assisted recombination of the device, the V_{OC} and J_{SC} were tested as a function of the solar simulator illumination intensity (0.10, 0.16, 0.32, 0.50, 0.63, 0.79, 1.00 sun). As shown in Fig. 5c, the relationship between the V_{OC} and the logarithm of different incident light intensities is linear.[26]

$$\frac{\partial V_{OC}}{\partial(\ln I)} = \frac{nKT}{q} \quad (1)$$

Among them, I, K, T, q, and n represent the light intensity, Boltzmann constant, absolute temperature, fundamental charge, and ideal factor, respectively. When the slope of the fitted line approaches 1 KT/q, it indicates that trap-assisted recombination in the device can be ignored. As shown in Fig. 5c, the slope value of the PEDOT:PSS device is 1.35 KT/q, whereas the slope value of the CsCl-PEDOT:PSS device is 1.32 KT/q. This result indicates that trap-assisted recombination is effectively suppressed in the CsCl PEDOT:PSS device, promoting charge extraction. As shown in Fig. 5d, on the logarithmic scale, there is a linear relationship between the J_{SC} and different incident light intensities ($J_{SC} \propto I^{\alpha}$).[27] The efficiency of the device is close to 1, indicating that the bimolecular recombination of the device can be ignored. The α of the PEDOT:PSS device is 1.0594, and the α of the CsCl-PEDOT:PSS device is 1.02979. In PEDOT:PSS devices, a higher α value suggests that the space charge effect within CsCl-PEDOT:PSS devices is suppressed.

The *J–V* characteristic curves of PSS devices under dark conditions based on PEDOT:PSS and CsCl-PEDOT:PSS are shown in Fig. 5e. The device based on CsCl-PEDOT:PSS has a significantly lower dark current density in the low voltage region compared to the original device, indicating that the doping of CsCl suppresses leakage current and improves carrier transport efficiency. Further research was conducted on the doping of CsCl to analyze the defect density of perovskite thin films. SCLC tests were performed on pure hole devices ITO/PEDOT:PSS/$MAPbI_{3-x}Cl_x$/PTAA/Ag and ITO/CsCl-PEDOT:PSS/$MAPbI_{3-x}Cl_x$/PTAA/Ag, as shown in Fig. 5f. The density of defect states in PSCs can be calculated using the following formula:[28]

$$N_{trap} = \frac{V_{TEL}(2\varepsilon_r\varepsilon_0)}{ed^2} \quad (2)$$

V_{TEL} represents the maximum voltage at which traps are filled, d is the film thickness, ε_0 is the vacuum dielectric constant, e is the electron charge, and ε_r is the dielectric constant. A higher V_{TEL} means a higher trap density. The defect-filling voltage based on the PEDOT:PSS device is 1.14 V, and the defect state-filling voltage of the CsCl-PEDOT:PSS device is 0.88 V, indicating that perovskite is deposited on CsCl-PEDOT:PSS and the defect state density between interfaces is lower. The lower density of defect states is also a direct result of the larger grain size of the perovskite, which can improve the FF.

The devices doped with CsCl PEDOT:PSS as an HTL exhibit improved photoelectric performance and enhanced stability. As shown in Fig. S4 (ESI†), the complete device ITO/PEDOT:PSS/$MAPbI_{3-x}Cl_x$/PCBM/BCP/Ag was prepared and packaged in a nitrogen-atmosphere glove box. The long-term stability of the CsCl-PEDOT:PSS device and PEDOT:PSS device was measured. After 400 hours, PEDOT:PSS devices maintain 86% of their original efficiency, while CsCl-PEDOT:PSS devices maintain 92% of their original efficiency. In addition, we have applied CsCl-PEDOT:PSS as an HTL in $(FASnI_3)_{0.6}(MAPbI_3)_{0.4}$ PSCs. The ITO/CsCl-PEDOT:PSS/$(FASnI_3)_{0.6}(MAPbI_3)_{0.4}$/PCBM/BCP/Ag device as shown in Fig. 6a was prepared. The *J–V* curve is shown in Fig. 6b, and the performance parameters are shown in Table S2 (ESI†). The PCE is increased from 19.49% to 21.44%, the V_{OC} is increased from 0.854 V to 0.856 V, the short circuit current is increased from 31.630 mA cm^{-2} to 32.925 mA cm^{-2}, and the FF is increased from 72.20% to 76.03%. Therefore, CsCl doped PEDOT:PSS as an HTL can be used not only in $MAPbI_{3-x}Cl_x$ PSCs but also in $(FASnI_3)_{0.6}(MAPbI_3)_{0.4}$ PSCs.

4 Conclusion

In conclusion, CsCl doping in PEDOT:PSS reduces the roughness of CsCl-PEDOT:PSS films, which is conducive to the density and grain growth of perovskite films deposited on it, and improves the quality of the films. The application of CsCl-doped PEDOT:PSS as an HTL in PSCs effectively increases the composite resistance, reduces carrier recombination, and improves the charge transport capacity. Through dark current

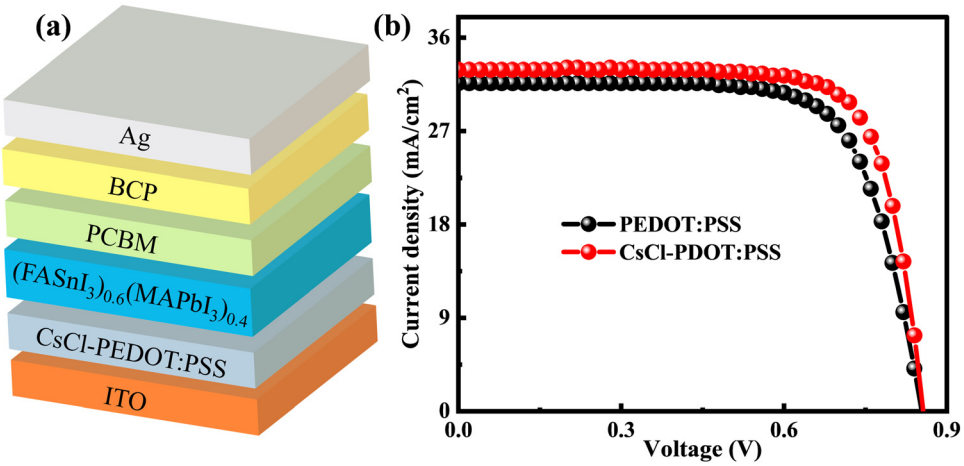

Fig. 6 (a) Device structure and (b) J–V curve of the $(FASnI_3)_{0.6}(MAPbI_3)_{0.4}$ perovskite.

and space charge limited current, it can be concluded that CsCl doping in PEDOT:PSS can reduce defect-assisted recombination and inhibit the leakage current of the device, and the defect state density between the interfaces is low. The larger perovskite grain size also directly results in a lower density of defect states, which can enhance the FF. At the same time, cesium chloride-doped PEDOT:PSS is used as an HTL in $(FASnI_3)_{0.6}(MAPbI_3)_{0.4}$ PSCs, PSCs with the device structure of ITO/CsCl-PEDOT:PSS/$(FASnI_3)_{0.6}(MAPbI_3)_{0.4}$/PCBM/BCP/Ag were prepared, and the PCE increased from 19.49% to 21.44%. Therefore, CsCl doping of PEDOT:PSS as the HTL improved the conductivity. To achieve high efficiency and stability, PSCs provide a new effective strategy.

Data availability

Experimental data will be provided as required.

Conflicts of interest

The authors declare that they have no known competing financial interests or personal relationships that could have appeared to influence the work reported in this paper.

Acknowledgements

This work was supported by the Natural Science Foundation of Chongqing (grant no. cstc2021jcyj-msxmX0576), the Science and Technology Research Program of Chongqing Municipal Education Commission (grant no. KJQN202200518), the National Natural Science Foundation of China (grant no. 12264060), the Scientific Research Foundation of Guizhou Province Education Ministry (grant no. QJHKYZ[2020]037), and the Doctoral Research Foundation of Zunyi Normal College (grant no. ZS-BS[2021]09).

References

1 G. Liu, X. Xie, X. Xu, Y. Wei, F. Zeng and Z. Liu, High-performance inverted two-dimensional PSCs using non-fullerene acceptor as the electron transport layer, *Org. Electron.*, 2018, **62**, 189–194.
2 Y. Noh, J. Jeong, S. Kim, H.-K. Kim and S.-I. Na, Non-fullerene-based small molecules as an efficient n-type electron transporting layers in inverted organic-inorganic halide PSCs, *J. Ind. Eng. Chem.*, 2018, **65**, 406–410.
3 F. M. Rombach, S. A. Haque and T. J. Macdonald, Lessons learned from spiro-OMeTAD and PTAA in PSCs, *Energy Environ. Sci.*, 2021, **14**, 5161–5190.
4 Y. C. Chin, M. Daboczi, C. Henderson, J. Luke and J. S. Kim, Suppressing PEDOT: PSS Doping-Induced Interfacial Recombination Loss in Perovskite Solar Cells, *ACS Energy Lett.*, 2022, **7**, 560–568.
5 D. Xu, Z. Gong, Y. Jiang, Y. Feng, Z. Wang, X. Gao, X. Lu, G. Zhou, J. M. Liu and J. Gao, Constructing molecular bridge for high-efficiency and stable perovskite solar cells based on P3HT, *Nat. Commun.*, 2022, **13**, 7020.
6 S. Jung, S. Choi, W. Shin, H. Oh, J. Oh, M. Y. Ryu, W. Kim, S. Park and H. Lee, Enhancement in Power Conversion Efficiency of Perovskite Solar Cells by Reduced Non-Radiative Recombination Using a Brij C_{10}-Mixed PEDOT: PSS Hole Transport Layer, *Polymers*, 2023, **15**, 772–785.
7 A. Jain, P. Subudhi, G. M. Khanal and D. Punetha, Simulation-Based Analysis of Environmentally Friendly Perovskite Solar Cells: Projecting 21.61% Efficiency with Lead-Free $CsSn_{0.5}Ge_{0.5}I_3$, *Phys. Status Solidi*, 2025, **222**(6), 2400727.
8 L. Chen, C. Li, Y. Xian, S. Fu, A. Abudulimu, D. B. Li, J. D. Friedl, Y. Li, S. Neupane, M. S. Tumusange, N. Sun, X. Wang, R. J. Ellingson, M. J. Heben, N. J. Podraza, Z. Song and Y. Yan, Incorporating Potassium Citrate to Improve the Performance of Tin-Lead Perovskite Solar Cells, *Adv. Energy Mater.*, 2023, **13**, 2301218.
9 P. Guo, J. Dong, C. Xu, Y. Yao, J. You, H. Bian, W. Zeng, G. Zhou, X. He, M. Wang, X. Zhou, M. Wang and Q. Song, Fabrication of an ultrathin PEG-modified PEDOT: PSS HTL for high-efficiency Sn–Pb perovskite solar cells by an eco-friendly solvent etching technique, *J. Mater. Chem. A*, 2023, **11**, 7246–7255.

10 P. Yadav, P. Subudhi, H. Dixit and D. Punetha, Numerical optimization of cesium bismuth iodide-based CIGS/Perovskite tandem solar cells for enhanced photovoltaic performance, *Opt. Laser Technol.*, 2025, **182**, 112072.
11 A. Pradhan, P. Subudhi and D. Punetha, Enhancing photovoltaic performance in copper-based perovskites: A comparative analysis of 3D and 2D structural paradigms for superior efficiency, *J. Power Sources*, 2025, **629**, 235999.
12 A. Alexander, A. B. Pillai, V. K. Pulikodan, A. Joseph, A. M. Raees and M. A. G. Namboothiry, Hydrophobic poly-TPD modified PEDOT PSS surface for improved and stable photovoltaic performance of $MAPbI_3$ based p-i-n perovskite solar cells, *J. Appl. Phys.*, 2023, **134**, 085002.
13 S. Ma, Y. Bai, H. Wang, H. Zai, J. Wu, L. Li, S. Xiang, N. Liu, L. Liu, C. Zhu, G. Liu, X. Niu, H. Chen, H. Zhou, Y. Li and Q. Chen, 1000 h Operational Lifetime Perovskite Solar Cells by Ambient Melting Encapsulation, *Adv. Energy Mater.*, 2020, **10**, 1902472.
14 L. Chen, C. Xu, W. Hu, Y. Yao, L. Niu, G. Xu, Y. Zhong, P. Guo and Q. Song, Improving the electrical performance of inverted perovskite solar cell with LiF anode buffer layer, *Org. Electron.*, 2022, **101**, 106401.
15 H. Dixit, D. Punetha and S. K. Pandey, Comparative Study and Analysis of Different Perovskite Solar Cells with Inverted Architecture, *Comput. Math. Nanoelectron. Astrophys.*, 2021, **342**, 125–135.
16 Seri Lee Doo-Hwan Kim, Gyu Min Kim and Se. Young Oh Physical, Effects of 2PACz Layers as Hole-Transport Material on the Performance of Perovskite Solar Cell, *Electron. Mater. Lett.*, 2023, **19**, 510–517.
17 X. Zhao, S. Zhong, S. Wang, S. Li and S. Wu, Potassium thiocyanate additive for PEDOT: PSS layer to fabricate efficient tin-based perovskite solar cells, *Int. J. Miner., Metall. Mater.*, 2023, **30**, 2451–2458.
18 A. G. Al-Gamal, A. M. Elseman, M. Abdel-Shakour, T. H. Chowdhury, K. I. Kabel, A. A. Farag, A. M. Rabie, N. E. A. AbdEl-Sattar, N. Fukata and A. Islam, Synergistic effect of integrating N-functionalized graphene and PEDOT: PSS as hole transporter bilayer for high-performance perovskite solar cells, *Adv. Compos. Hybrid Mater.*, 2023, **6**, 103.
19 T. Kong, J. Song, Y. Zhang, E. L. Lim, X. Liu, W. Tress, D. Bi and A. Newly Crosslinked-double, Network PEDOT: PSS@PEGDMA toward Highly-Efficient and Stable Tin-Lead Perovskite Solar Cells, *Small*, 2023, **19**, 2303159.
20 S. Sandrez and Z. Molenda, Cl. Guyot, O. Renault, J.P. Barnes, L. Hirsch, T. Maindron, G. Wantz1. Halide Perovskite Precursors Dope PEDOT: PSS, *Adv. Electron. Mater.*, 2021, 7(9), 2100394.
21 X. Zhao, S. Zhong, S. Wang, S. Li and S. Wu, Potassium thiocyanate additive for PEDOT: PSS layer to fabricate efficient tin-based perovskite solar cells, *Int. J. Miner., Metall. Mater.*, 2023, **30**, 2451–2458.
22 Y. Yang, Y. Yao, Y. Li, X. Zhao, W. Cheng, B. Chen, L. Chen, P. Li and S. Tang, Application of arginine-doped PEDOT: PSS as a hole transfer layer in perovskite solar cells, *J. Mater. Chem. C*, 2023, **11**, 13814–13823.
23 X. Tang, M. Chen, L. Jiang, M. Li, G. Tang and H. Liu, Improvements in efficiency and stability of perovskite solar cells using a cesium chloride additive, *ACS Appl. Mater. Interfaces*, 2022, **14**, 26866–26872.
24 A. Kumar, N. Pandey, D. Punetha and R. Saha, S. Chakrabarti. Tuning the structural and photophysical behavior of non-toxic $CsSnCl_3$ using reduced graphene oxide for optoelectronic applications, *Phys. Simul. Optoelectron. Devices*, 2023, 124150M.
25 A. Kumar, N. Pandey, D. Punetha, R. Saha, S. Choudhary and S. Chakrabarti, Reduced graphene oxide (rGO)-$CsSnI_3$ nanocomposites: a cost-effective technique to improve the structural and optical properties for optoelectronic device applications, *Organic, Hybrid, Perovskite Photovoltaics*, 2023, 126600B.
26 X. Li, Y. Tang, B. Song, F. Meng, C. Gao, L. Qin, Y. Hu, Z. Lou, F. Teng and Y. Hou, Efficient Tin-Based Perovskite Solar Cell with a Cesium Acetate Pre-buried PEDOT: PSS Hole Transport Layer, *J. Phys. Chem. Lett.*, 2024, **15**, 1355–1362.
27 N. Cheng, Z. Liu, Z. Yu, W. Li, Z. Zhao, Z. Xiao, B. Lei, S. Sun and W. Zi, High performance inverted perovskite solar cells using PEDOT: PSS/KCl hybrid hole transporting layer, *Org. Electron.*, 2021, **98**, 106298.
28 Y. Li, B. Shi, Q. Xu, L. Yan, N. Ren, Y. Li, W. Han, Z. Zhu, Y. Zhang, J. Liu, C. Sun, S. Wang, Q. Huang, D. Zhang, H. Ren, X. Du, Y. Zhao and X. Zhang, CsCl induced efficient fully-textured perovskite/crystalline silicon tandem solar cell, *Nano Energy*, 2024, **122**, 109285.